JASS Journal of Astronomy and Space Sciences

Nonthermal Radiation from Supernova Remnant Shocks

Hyesung Kang[†]

Department of Earth Sciences, Pusan National University, Pusan 609-735, Korea

Most of high energy cosmic rays (CRs) are thought to be produced by diffusive shock acceleration (DSA) at supernova remnants (SNRs) within the Galaxy. Fortunately, nonthermal emissions from CR protons and electrons can provide direct observational evidence for such a model and place strong constraints on the complex nonlinear plasma processes in DSA theory. In this study we calculate the energy spectra of CR protons and electrons in Type Ia SNRs, using time-dependent DSA simulations that incorporate phenomenological models for some wave-particle interactions. We demonstrate that the time-dependent evolution of the self-amplified magnetic fields, Alfvénic drift, and escape of the highest energy particles affect the energy spectra of accelerated protons and electrons, and so resulting nonthermal radiation spectrum. Especially, the spectral cutoffs in X-ray and γ-ray emission spectra are regulated by the evolution of the highest energy particles, which are injected at the early phase of SNRs. Thus detailed understandings of nonlinear wave-particle interactions and time-dependent DSA simulations of SNRs are crucial in testing the SNR hypothesis for the origin of Galactic cosmic rays.

Keywords: cosmic rays, supernova remnants, shock waves, nonthermal radiation

1. INTRODUCTION

Blast waves driven by supernova (SN) explosions are presumed to accelerate cosmic rays (CRs) at least to the first knee of $10^{15.3}$ eV and possibly up to the second knee of $10^{17.5}$ eV. Moreover, in terms of energy budget, Galactic SN luminosity, $L_{SN} \approx 10^{42}$ erg s^{-1}, is powerful enough to replenish escaping cosmic rays with a luminosity of $L_{CR} \approx 10^{41}$ erg s^{-1} (Blanford & Eichler 1987, Reynolds 2008). Time-dependent, diffusive shock acceleration (DSA) simulations of the CR acceleration at supernova remnants (SNRs) have demonstrated that an order of 10% of the SN explosion energy can be transferred to CRs, if a fraction $\gtrsim 10^{-4}$ of incoming thermal particles are injected into the CR population at the forward shock (e.g., Berezhko et al 2009, Kang 2010).

In DSA theory, CR particles are scattered by magneto-hydrodynamic (MHD) fluctuations (plasma waves) and gain energy through multiple crossings of the shock (Bell 1978, Drury 1983). Some suprathermal particles with velocities large enough to swim against the downstream MHD turbulence can return across the shock and get injected into the Fermi process (Malkov & Drury 2001, Kang et al. 2002). Then those streaming CRs excite resonant Alfvén waves via two-stream instability and nonresonant waves via CR current-driven instability, which in turn amplify turbulent magnetic fields in the preshock region (Bell 1978, Lucek & Bell 2000, Bell 2004). Furthermore, magnetic fluctuations on scales larger than the CR gyroradius can grow in the presence of short-scale, circularly-polarized Alfvén waves (Bykov et al. 2011, Rogachevskii et al. 2012) and through the firehose, filamentation, and acoustic instabilities (see Schure et al. 2012 for a review). Amplification of turbulent magnetic fields via plasma instabilities and injection of CRs via wave-particle interactions are regarded as integral ingredients of DSA at collisonless shocks.

X-ray observations of thin rims at the forward shock of several SNRs can be explained by the acceleration of ~10-100 TeV electrons, which cool radiatively in several 100 μG magnetic fields (e.g., Bamba et al 2003, Parizot et al. 2006, Reynolds et al 2012). This provides convincing evidence for efficient magnetic field amplification at strong CR modified
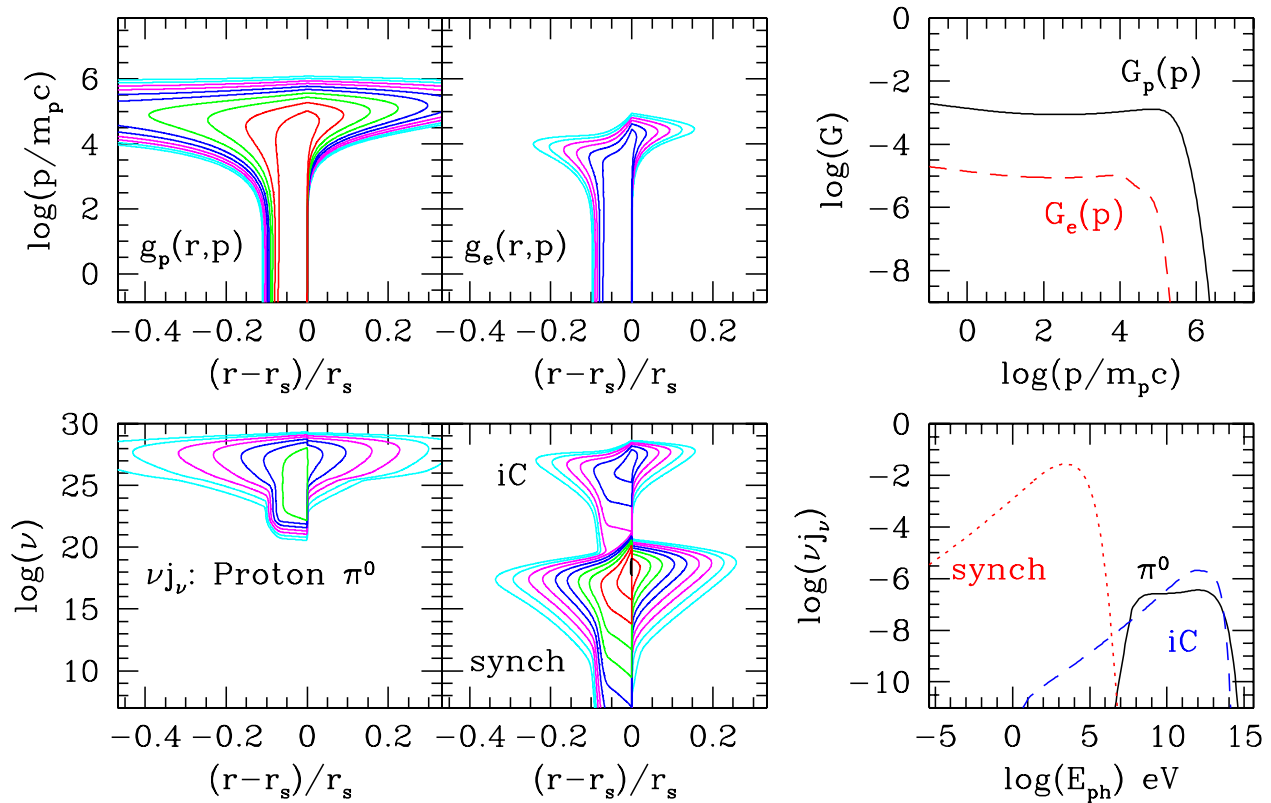
Fig. 1. DSA simulation results of a Sedov blast wave from Type Ia supernova (see text for the model parameters). *Left four panels*: Proton and electron distribution functions, $g_p(r,p) = f_p \cdot p^4$ and $g_e(r,p) = f_e \cdot p^4$, respectively, p-p secondary π^0 decay emissivity, $vj_v(r,v)$, and electron synchrotron and iC emissivity, $vj_v(r,v)$ are shown. Contour intervals are a factor of 10. *Right two panels*: Volume integrated energy spectra, $G_p(p)$ (solid line) and $G_e(p)$ (dashed), for protons and electrons, respectively, the volume integrated radiation spectra of π^0 decay (solid), synchrotron (dotted), and iC scattered (dashed) emissivities (where $K_{e/p} = 10^{-2}$ is adopted). The results are shown at the age of 255 years.

shocks. If the magnetic fields are amplified to ~30 μG in the upstream region of SNRs, CR ions of charge number Z might gain energies up to $E_{max} \sim 10^{15.5}$ Z eV, which may explain the all-particle CR spectrum up to the second knee at ~$10^{17.3}$ eV with rigidity-dependent cutoffs (Hillas 2005).

Recent γ-ray observations of several SNRs in GeV-TeV bands can be interpreted by a combination of decay of neutral pions produced in nuclear interactions between CR protons and the ambient medium and inverse Compton (iC) scattering of the background radiation by CR electrons (Acciari et al. 2011, Giordano et al. 2012, Morlino & Caprioli 2012). Fig. 1 shows the results of a DSA simulation of Type Ia SNR for the following parameters: the ejecta mass, $M_{ej} = 1.4$ $M_\odot$, the SN explosion energy, $E_o = 10^{51}$ ergs, the hydrogen number density, $n_{H,0} = 0.3$ cm³, the gas temperature, $T_0 = 3$ $\times 10^4$ K, and the constant magnetic field strength, $B_0 = 30$ μG for the background flow (Kang et al. 2012). The proton to electron number ratio is assumed to be $K_{e/p} = 10^{-2}$ in the right panels. One can see that the spatial and spectral distribution of protons ($g_p = f_p p^4$) and electrons ($g_e = f_e p^4$)

behave differently because of electronic synchrotron and iC energy losses. The distribution of nonthermal emissions depends on the magnetic field strength and the background density in addition to f_p and f_e. Obviously, the importance of π^0 decay relative to electron iC emissions should scale with $n_{H,0}/K_{e/p}$, once the energy spectra of CR protons and electrons and the background radiation field are given. So multi-band observations of nonthermal emissions from SNRs can be used to explore the complex nonlinear plasma processes in the DSA theory.

In fact, steep γ-ray photon spectra of $N(E_v) \propto E_v^{-\Gamma}$ with $\Gamma \sim$ 2.2-2.4 GeV band, observed in several young SNRs, may not be consistent with the spectra of CR protons and electrons predicted from nonlinear DSA modeling of SNRs (Abdo 2010, Acciari et al. 2011, Caprioli 2011). Another observational evidence indicating a soft source CR spectrum comes from the measurements of CR nuclei at Earth up to ~10^{14} eV by TRACER, whose flux spectrum can be fitted by $J(E) \propto E^{-2.67}$ (Ave et al. 2009). If the mean propagation path length of CRs scales with the particle energy as $\Lambda \propto$

$E^{-0.6}$, as commonly adopted, the source spectrum, $N(E) \propto E^{-\alpha}$ with $\alpha \sim 2.3$-2.4, is preferred. However, if order of 10% of the SN explosion energy is to be transferred to CRs, the flow structure could be significantly modified by the CR pressure, resulting in a concave particle spectrum which is harder than the test-particle power-law of E^{-2} for E $\gg 1$ GeV (Berezhko et al 2009, Edmon et al. 2011). Presumably, these discrepancies call for a substantial revision of the standard nonlinear DSA at strong shocks (Kang 2010, Caprioli 2012). Thus in order to reconcile the DSA predictions with these observations, the DSA efficiency at typical SNRs should not be much higher than 10% and the energy spectrum of shock accelerated particles should be softer than the canonical test-particle power-law. One way to soften the CR spectrum is to include fast Alfvénic drift in the shocks precursor, which reduces the velocity jumps that CRs experience across the shock (Caprioli 2012, Zirakashvili & Ptuskin 2008, 2012). We will explore this issue using our numerical simulations below.

2. DSA MODELS AND SIMULATIONS

Here we consider the CR acceleration at quasi-parallel shocks where the magnetic field lines are parallel to the shock normal. We solve the following diffusion-convection equation (Skilling 1975):

$$\frac{\partial g}{\partial t} + (u + u_w) \frac{\partial g}{\partial r} = \frac{1}{3r^2} \frac{\partial}{\partial r} \left[r^2 (u + u_w) \right] \left(\frac{\partial g}{\partial y} - 4g \right)$$
$$+ \frac{1}{r^2} \frac{\partial}{\partial r} \left[r^2 \kappa(r,y) \frac{\partial g}{\partial r} \right] + p \frac{\partial}{\partial y} \left(\frac{b}{p^2} g \right), \quad (1)$$

where $g = f(r,p,t) \cdot p^4$ is the isotropic part of the pitch-angle averaged CR distribution function, $y = \ln (p/m_p c)$, and $\kappa(r,y)$ is the spatial diffusion coefficient parallel to the mean magnetic field. The velocity u_w represents the effective relative motion of scattering centers (MHD turbulences) with respect to the bulk flow velocity, u. The basic gas dynamic equations and details of the spherical Cosmic-Ray Amr Shock (CRASH) code can be found in Kang & Jones (2006).

The electronic synchrotron/iC cooling constant is defined as $b(p) = -dp/dt = (4 e^4/9 m_e^4 c^6) B_e^2 p^2$ in cgs units, where e and m_e are electron charge and mass, respectively. The effective magnetic energy density, $B_e^2 = B^2 + B_r^2$, includes the energy density of the ambient radiation field, $B_r = 6.5 \mu G$, which combines the cosmic background and mean Galactic radiation fields (Edmon et al. 2011). The cooling term for protons is set to be $b(p) = 0$.

Thermal Leakage Injection: In order for suprathermal particles to leak upstream across the shock transition layer, whose thickness is order of the gyroradius of downstream thermal protons, the particle speed must be several times larger than the downstream flow speed, u_2. So injection of protons and electrons from the postshock thermal pool into the CR population via wave-particle interactions are emulated by a phenomenological model, in which particles above an 'effective' injection momentum, $p_{inj} \approx 6.6 \, m_p u_2$, are allowed to cross the shock upstream (Kang et al. 2002). This injection model results in the injected particle fraction, $\xi = n_{cr,2} / n_2$, that ranges from 10^{-5} to $10^{-3.5}$ and decreases in time as the shock slows down. Protons and electrons of the same rigidity ($R = pc/Ze$) are injected in the same manner in the simulations.

Magnetic Field Amplification: CRs streaming upstream in the shock precursor generate both resonant Alfvén waves (Bell 1978, Lucek & Bell 2000) and nonresonat waves (Bell 2004), and in turn amplify the turbulent magnetic fields by orders of magnitude. As mentioned in Introduction, several plasma and MHD simulations have shown that both $B_{\parallel}/B_0$ and $B_{\perp}/B_0$ can increase by a factor of up to $\sim$10-45 via CR streaming instabilities (e.g., Riquelme & Spitkovsky 2009, 2010, Guo et al. 2010, Gargate & Spitkovsky 2012, Rogachevskii et al. 2012). Furthermore, there are several other instabilities that may amplify the turbulent magnetic fields on scales greater than the CR gyroradius (Schure et al. 2012). Here, we adopt the prescription for MFA due to CR streaming instabilities that was suggested by Caprioli (2012), based on the assumption of isotropization of the amplified magnetic fields. In the upstream region ($r > R_s$),

$$\frac{B(r)^2}{B_0^2} = 1 + (1 - \omega_H) \cdot \frac{4}{25} M_{A,0}^2 \frac{\left(1 - U(r)^{5/4}\right)^2}{U(r)^{3/2}}, \quad (2)$$

where $M_{A,0} = u_s(t)/V_{A,0}$ is the Alfvénic Mach number for the instantaneous shock speed with respect to the far upstream Alfvén speed, $V_{A,0} = B_0 / \sqrt{4\pi\rho_0}$, and $U(r) = [u_s - u(r)]/u_s$ is the flow speed in the shock rest frame normalized by the shock speed. The factor $(1-\omega_H)$ accounts for loss of the magnetic field energy due to wave dissipation (see below).

Alfvénic Drift: The magnetic field fluctuations generated by CR streaming instabilities drift with respect to the underlying flow in the shock precursor (Skilling 1975). In the upstream region, the mean drift speed of scattering centers is assumed to be the Alfvén speed along the parallel magnetic field, $u_w(r) = +V_A = +B_{\parallel} / \sqrt{4\pi\rho}$, pointing away from the shock. As mentioned above, the amplified magnetic fields are likely to be nearly isotropized by various

Table 1. Model Parameters.

Name	$n_{H,0}$ (cm^{-3})	T_0 (K)	r_o (pc)	t_o (yr)	f_A	ω_H	ζ	$u_{w,2}$
SNR1	0.3	3×10^4	3.18	255.	1.0	0.5	0.1	0
SNR2	0.3	3×10^4	3.18	255.	1.0	0.5	0.5	0
SNR3	0.3	3×10^4	3.18	255.	0.1	0.5	0.1	0
SNR4	0.3	3×10^4	3.18	255.	1.0	0.5	0.1	$-V_A$

instabilities, so the effective Alfvén speed could be defined by the local amplified field $B(r)$ given by Eq. (2) In order to consider the uncertainty in the model, we set the local Aflvén speed as

$$V_A(r) = \frac{B_0 + (B(r) - B_0) f_A}{\sqrt{4\pi\rho(r)}}, \qquad (3)$$

where f_A is a free parameter that ranges 0.1-1.0 (Zirakashvili & Ptuskin 2008, Lee et al. 2012). In the postshock region, the Alfvénic turbulence is nearly isotropic in planar shocks, so the drift is expected to be $u_{w,2} \approx 0$ (Jones 1993). For spherical Sedov-Taylor blast waves, however, the CR pressure decreases behind the shock, so Alfvén wave may drift inward with $u_{w,2} \approx -V_A$ downstream of the shock. We will consider the models with both upstream and downstream drift (SNR4 model).

Wave Dissipation and Precursor Heating: In the late Sedov-Taylor stage, the magnetic turbulence can dissipate due to nonlinear wave-wave interactions and ion-neutral collisions (Ptuskin & Zirakashvili 2005). Gas heating due to the Alfvén wave dissipation in the precursor is prescribed by the following term:

$$W(r,t) = -\omega_H \cdot V_A(r) \frac{\partial P_c}{\partial r}, \qquad (4)$$

where P_c is the CR pressure. The parameter ω_H is introduced to control the degree of wave dissipation and a fiducial value of $\omega_H = 0.5$ is adopted. For larger values of ω_H, of course, the magnetic field amplification is suppressed (see Eq. (4)).

Free Escape Boundary: The magnetic turbulence on scales of the gyroradius of the highest energy CR protons may not provide sufficient scattering to confine those particles around the shock. In order to account for escape of the protons near $p_{p,max}$, we implement a free escape boundary (FEB) at an upstream location by setting $f_{(rFEB,p)}=0$ at $r_{FEB}=(1+\zeta)r_s(t)$ where $\zeta=0.1-0.5$. This FEB condition can mimic escape of the highest energy particles with a diffusion length, $\kappa(p)/u_s(t)>\zeta r_s(t)$. Since the shock speed decreases while the shock radius increases in time, with this FEB the mean momentum of escaping particles decreases as $<p_{esc}> \propto t^{-1/5}$.

Sedov-Taylor Self-Similar Solution: Here we consider a Type Ia supernova explosion with the ejecta mass, $M_{ej} = 1.4$ $M_\odot$, and the explosion energy, $E_o = 10^{51}$ ergs. The background ISM is characterized by $n_H = 0.3$ cm^{-3} and $T_0 = 3 \times 10^4$ K, and assumed to be completely ionized with the mean molecular $\mu = 0.61$. The background magnetic field strength is set to be $B_0 = 5$ μG, so the Alfvén speed is $V_{A,0} = 16.8$ km s^{-1} and the Alfvénic Mach number is $M_A \approx 180 \, (u_s/3000$ km s$^{-1})$. The rest of models parameters are summarized in Table 1. We consider SNR1 model as a fiducial case. The effects of FEB are explored by SNR2 model with $\zeta = 0.5$. In SNR3 model, Alfvén speed is reduced by setting $f_A = 0.1$. SNR4 model includes the effects of Alfvénic drift in the downstream region, i.e., $u_{w,2}=-V_A(r)$. In all four models, the wave drift speed in the upstream region is set to be $u_{w,1} = +V_A (r)$.

For a Type Ia SNR, the highest proton energy ($p_{p,max}$) is achieved at the beginning of the Sedov-Taylor (ST) stage and the transfer of explosion energy to the CR component occurs mostly during the early ST stage. In order to account for the CR acceleration from free expansion stage through ST stage, we begin the calculations with the ST similarity solution at $t/t_o = 0.2$ and follow the evolution of the forward shock during the early ST stage up to $t/t_o =10$. We will show below the energy conversion to CRs saturates at ~30% after $t/t_o \gtrsim 10$.

3. DISCUSSION AND CONCLUSION

Fig. 2 shows the spatial profiles of the amplified magnetic field and the CR pressure, and the volume-integrated distribution functions of protons and electrons, $G_p(p) = 4\pi \int g_p(r,p)r^2 dr$ and $G_e(p) = 4\pi \int g_e(r,p)r^2 dr$, respectively, for models SNR1-SNR4. One can see that the spatial profile of B (r,t) has a smooth precursor, and the magnetic field strength decreases in time. For example, the postshock magnetic field strength is $B_2 \approx 200$-500 μG at the SNR age of $t \approx 255$ yr. These overall pictures seem to be consistent with the observations of young SNRs, which were discussed in Introduction.

Since the MFA factor scales with the degree of flow modification in the precursor (see Eq. (2)) and the diffusion length, $l_{diff} \propto p$, increases with the particle momentum, the low energy part of the CR spectrum is softened by Alfvénic drift much more than the high energy part (Kang 2012). As can be seen in the right panels of Fig. 2, the concave curvature in the energy spectra, G_p and G_e, does not disappear entirely even with Alfvénic drift, except in SNR4 model. The volume integrated electron energy spectrum steepens by one power of the momentum for $p > p_{e,br}/m_p c \approx$
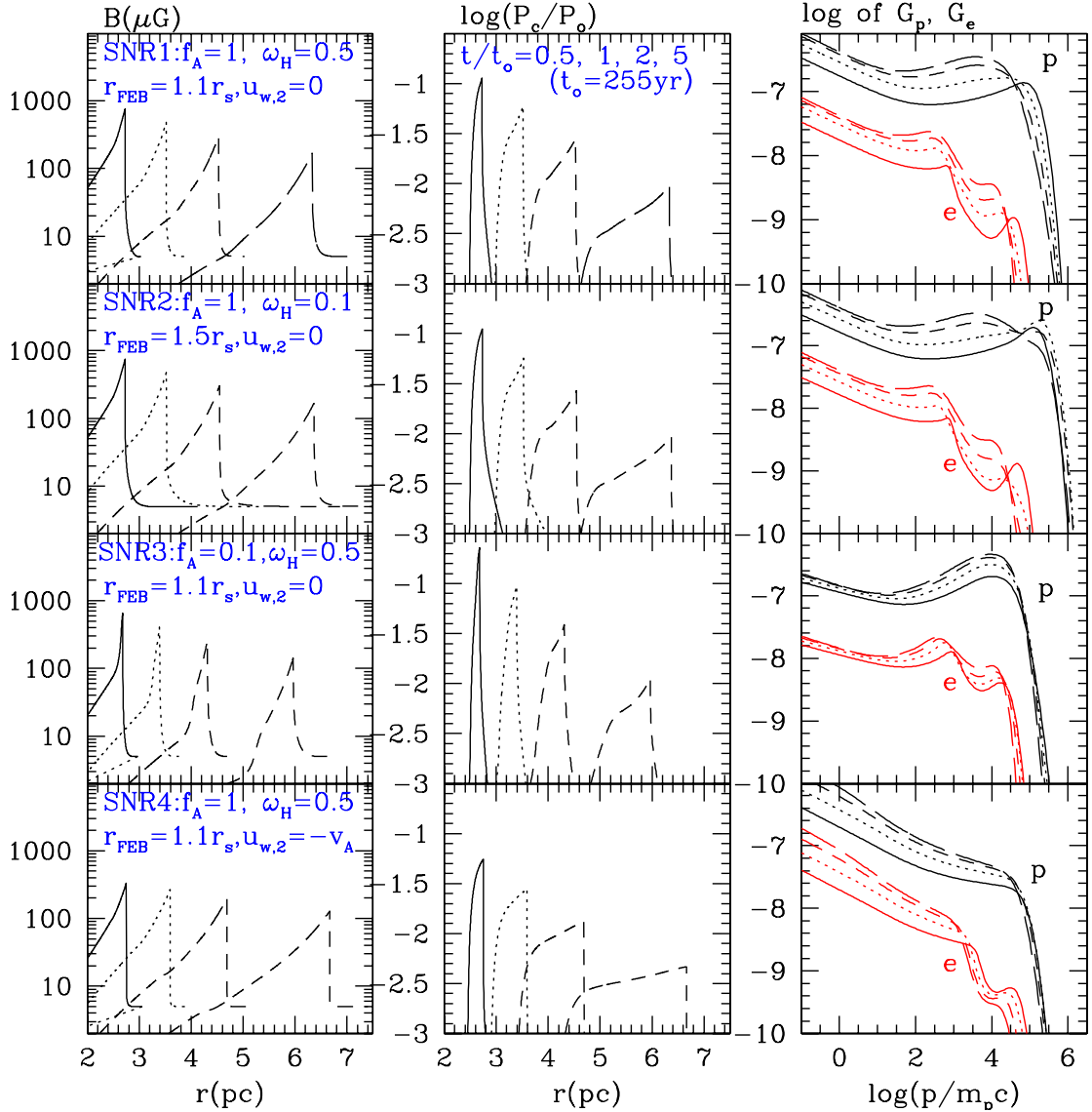
Fig. 2. Time evolution of SNR1-SNR4 models at $t/t_o = 0.51$ (solid lines), 1 (dotted), 2 (dashed) and 5 (long dashed), where $t_o = 255$ yr. See Table 1 for the model parameters and normalization constants. In the left column, the magnetic field structures are given in units of microgauss, while the CR pressure is expressed in terms of $P_o = \rho_o u_o^2$ in the middle column. In the right column the volume integrated distribution functions, $G_p(p)$ for protons (upper black curves) and $G_e(p)$ for electrons (lower red curves), are given in arbitrary units. Note that $K_{e/p} = 0.1$ is adopted here for clarity. The low energy part of the CR spectra is steepened preferentially by Alfvénic drift, but the high energy part is still harder than the canonical test-particle spectrum except for SNR4 model.

10^3 due to synchrotron/iC cooling. The peak in G_e near $p_{e,max}$ comes from the electron population in the upstream region, which cools much less efficiently due to weaker magnetic fields there.

Comparison of G_p and G_e in the four models demonstrates that the high energy cutoffs in the CR energy spectra depend on time evolution of $u_s(t)$ and $B(r,t)$ in addition to the model parameters for Alfvénic drift, wave damping, and FEB. In SNR4 model, in which the Alfvénic drift in the postshock region is included as well, the CR spectra are much softer, the postshock CR pressure is smaller by a factor of two or so,

compared to SNR1 model.

Fig. 3 compares how different energy components change in time: the kinetic energy, E_{kin}, thermal energy, E_{th}, and CR energy, E_c, expressed in units of E_o. The fraction of the explosion energy transferred to CRs asymptotes to 0.25-0.3 in these models, which should be sufficient to explain the CR luminosity of the Galaxy. In SNR3 model, the CR proton spectrum, G_p, is harder than that of other three models, and so more high energy particles escape from the shock, resulting in a greater energy loss, E_{esc} (green dot-dashed lines). We note that the CR energy (E_c) achieved

137
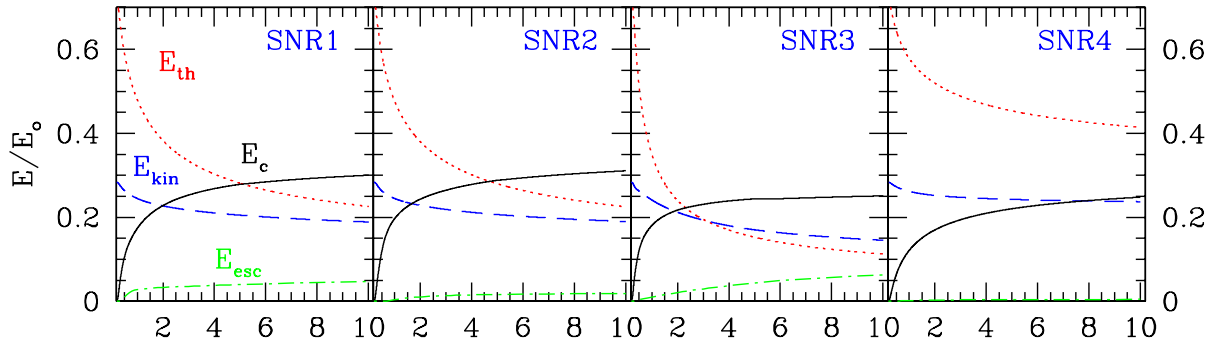
Fig. 3. Integrated thermal (E_{th}, red dotted lines), kinetic (E_{kin}, blue dashed lines), and CR (E_c, black solid lines) energies inside the simulation volume are shown in units of the explosion energy E_o. The green dot-dashed lines represent the fraction of energy carried by the highest energy protons escaped through the FEB. See Table 1 for the model parameters. The shock age is given in units $t_o = 255$ yr.

during Sedov-Taylor stage is similar in all four SNR models, although the CR proton and electron spectra depend sensitively on the details of DSA model, and behave rather differently (see Fig. 2).

In this study we have explored how wave-particle interactions and plasma instabilities govern nonlinear DSA and the resulting nonthermal emissions from SNRs. As demonstrated in Figure 1, the CR electron spectrum near the high energy cutoff determines the X-ray synchrotron emissions and the iC scattered emissions in GeV-TeV band. The former depends on the distribution and evolution of the magnetic fields, while the latter depends on the background radiation field. The γ-ray emissions due to π_0 decay depend on the CR proton spectrum and the background matter density. Of course, the CR energy spectra are regulated by the degree of MFA and radiative cooling (e.g., $p_{p,max}$ and $p_{e,max}$), and by particle escape due to lack of plasma waves on relevant scales. Thus we need to understand better wave-particle interactions at nonrelativistic collisionless shocks in order to make quantitative predictions for the CR spectra and nonthermal radiation spectrum due to those CRs.

ACKNOWLEDGMENTS

REFERENCES

Abdo AA, Ackermann M, Ajello M, Allafort A, Baldini L, et al., Fermi-Lat Discovery of GeV Gamma-Ray Emission from the Young Supernova Remnant Cassiopeia A, ApJ, 710, L92-L97 (2010). http://dx.doi.org/10.1088/2041-8205/710/1/L92

Acciari VA, Aliu E, Arlen T, Aune T, Beilicke M, et al., Discovery of TeV Gamma-ray Emission from Tycho's Supernova Remnant, ApJ, 730, L20-L25 (2011). http://dx.doi.org/10.1088/2041-8205/730/2/L20

Ave M, Boyle PJ, Hoeppner C, Marshall J, Mueller D, Propagation and source energy spectra of cosmic ray nuclei at high energies, ApJ, 697, 106-114 (2009). http://dx.doi.org/10.1088/0004-637X/697/1/106

Bamba A, Yamazaki R, Ueno M, Koyama K, Small-Scale Structure of the SN 1006 Shock with Chandra Observations, ApJ, 589, 827-837 (2003). http://dx.doi.org/10.1086/374687

Bell AR, The Acceleration of Cosmic Rays in Shock Fronts. I, MNRAS, 182, 147-156 (1978).

Bell AR, Turbulent amplification of magnetic field and diffusive shock acceleration of cosmic rays, MNRAS, 353, 550-558 (2004). http://dx.doi.org/10.1111/j.1365-2966.2004.08097.x

Berezhko EG, Ksenofontov LT, Voelk, HJ., Cosmic ray acceleration parameters from multi-wavelength observations. The case of SN 1006, A&A, 505, 169-176 (2009). http://dx.doi.org/10.1051/0004-6361/200911948

Blandford RD, Eichler D, Particle Acceleration at Astrophysical Shocks - a Theory of Cosmic-Ray Origin, Phys. Rept., 154, 1 (1987). http://dx.doi.org/10.1016/0370-1573(87)90134-7

Bykov AM, Osipov SM, Ellison DC, Cosmic ray current driven turbulence in shocks with efficient particle

acceleration: the oblique, long-wavelength mode instability, MNRAS, 410, 39-52 (2011). http://dx.doi.org/10.1111/j.1365-2966.2010.17421.x

Caprioli D, Understanding hadronic gamma-ray emission from supernova remnants, JCAP, 5, 26 (2011). http://dx.doi.org/10.1088/1475-7516/2011/05/026

Caprioli D, Cosmic-ray acceleration in supernova remnants: non-linear theory revised, JCAP, 7, 38 (2012). http://dx.doi.org/10.1088/1475-7516/2012/07/038

Drury LO'C, An Introduction to the Theory of Diffusive Shock Acceleration of Energetic Particles in Tenuous Plasmas, Rep. Prog. Phys., 46, 973-1027 (1983). http://dx.doi.org/10.1088/0034-4885/46/8/002

Edmon PP, Kang H, Jones TW, Ma R, Non-thermal radiation from Type Ia supernova remnants, MNRAS, 414, 3521-3536 (2011). http://dx.doi.org/10.1111/j.1365-2966.2011.18652.x

Gargaté L, Spitkovsky A, Ion Acceleration in Non-relativistic Astrophysical Shocks, ApJ, 744, 67-81 (2012). http://dx.doi.org/10.1088/0004-637X/744/1/67

Giordano F, Naumann MG, Ballet J, Bechtol K , Funk S, et al., Fermi Large Area Telescope Detection of the Young Supernova Remnant Tycho, ApJ, 744, L2-L6 (2012). http://dx.doi.org/10.1088/2041-8205/744/1/L2

Guo F, Jokipii JR, Kota J, Particle Acceleration by Collisionless Shocks Containing Large-scale Magnetic-field Variations, ApJ, 725, 128-133 (2010). http://dx.doi.org/10.1088/0004-637X/725/1/128

Hillas AM, TOPICAL REVIEW: Can diffusive shock acceleration in supernova remnants account for high-energy galactic cosmic rays?, J. Phys. G: Nucl. Part. Phys., 31, R95 (2005). http://dx.doi.org/10.1088/0954-3899/31/5/R02

Jones TW, Alfven wave transport effects in the time evolution of parallel cosmic-ray-modified shocks, ApJ, 413, 619-632, (1993). http://dx.doi.org/10.1086/173031

Kang H, Cosmic Ray Spectrum in Supernova Remnant Shocks, JKAS, 43, 25-39 (2010).

Kang H, Diffusive Shock Acceleration with Magnetic Field Amplification and Alfvenic Drift, JKAS, 45, 127-138 (2012).

Kang H, Edmon PP, Jones JW, Nonthermal Radiation from Cosmic-Ray Modified Shocks, ApJ, 745, 146-159 (2012). http://dx.doi.org/10.1088/0004-637X/745/2/146

Kang H, Jones TW, Numerical studies of diffusive shock acceleration at spherical shocks, Astropart. Phys, 25, 246-258 (2006). http://dx.doi.org/10.1016/j.astropartphys.2006.02.006

Kang H, Jones TW, Gieseler UDJ, Numerical Studies of Cosmic-Ray Injection and Acceleration, ApJ, 579, 337-

358 (2002). http://dx.doi.org/10.1086/342724

Lee S, Ellison DC, Nagataki S, A Generalized Model of Nonlinear Diffusive Shock Acceleration Coupled to an Evolving Supernova Remnant, ApJ, 750, 156-168 (2012). http://dx.doi.org/10.1088/0004-637X/750/2/156

Lucek SG, Bell AR, Non-linear amplification of a magnetic field driven by cosmic ray streaming, MNRAS, 314, 65-74 (2000). http://dx.doi.org/10.1046/j.1365-8711.2000.03363.x

Malkov MA, Drury LO'C, Nonlinear Theory of Diffusive Acceleration of Particles by Shock Waves, Rep. Progr. Phys., 64, 429-481 (2001). http://dx.doi.org/10.1088/0034-4885/64/4/201

Morlino G, Caprioli D, Strong evidence for hadron acceleration in Tycho's supernova remnant, Tycho, theoretical fit, Alfvén drift, A&A, 538, 81-94 (2012). http://dx.doi.org/10.1051/0004-6361/201117855

Parizot E, Marcowith A, Ballet J, Gallant YA, Observational Constraints on Energetic Particle Diffusion in Young Supernovae Remnants: Amplified Magnetic Field and Maximum Energy, A&A, 453, 387-395 (2006). http://dx.doi.org/10.1051/0004-6361/20064985

Ptuskin VS, Zirakashvili VN, On the spectrum of high-energy cosmic rays produced by supernova remnants in the presence of strong cosmic-ray streaming instability and wave dissipation, A&A, 429, 755-765 (2005). http://dx.doi.org/10.1051/0004-6361/20041517

Riquelme MA, Spitkovsky A, Nonlinear Study of Bell's Cosmic Ray Current-Driven Instability, ApJ, 694, 626-642 (2009). http://dx.doi.org/10.1088/0004-637X/694/1/626

Riquelme MA, Spitkovsky A, Magnetic Amplification by Magnetized Cosmic Rays in Supernova Remnant Shocks, ApJ, 717, 1054-1066 (2010). http://dx.doi.org/10.1088/0004-637X/717/2/1054

Reynolds SP, Supernova Remnants at High Energy, ARAA, 46, 89-126 (2008). http://dx.doi.org/10.1146/annurev.astro.46.060407.145237

Reynolds SP, Gaensler BM, Bocchino F, Magnetic Fields in Supernova Remnants and Pulsar-Wind Nebulae, Space Science Reviews, 166, 231-261 (2012). http://dx.doi.org/10.1007/s11214-011-9775-y

Rogachevskii I, Kleeorin N, Brandenburg A, Eichler D, Cosmic-Ray current-driven turbulence and mean-field dynamo effect, ApJ, 753, 6-22 (2012). http://dx.doi.org/10.1088/0004-637X/753/1/6

Schure KM, Bell AR, Drury LO'C, Bykov AM, Diffusive Shock Acceleration and Magnetic Field Amplification, Space Sci. Rev., 173, 491-519 (2012). http://dx.doi.org/10.1007/s11214-012-9871-7

Skilling J, Cosmic Ray Streaming. I - Effect of Alfvén Waves on Particles, MNRAS, 172, 557-566 (1975).

Zirakashvili VN, Ptuskin VS, Diffusive Shock Acceleration with Magnetic Amplification by Nonresonant Streaming Instability in Supernova Remnants, ApJ, 678, 939-949 (2008). http://dx.doi.org/10.1086/529580

Zirakashvili VN, Ptuskin VS, Numerical simulations of diffusive shock acceleration in SNRs, Astropart. Phys., 39, 12-21 (2012). http://dx.doi.org/10.1016/j.astropartphys.2011.09.003